Development and Analysis of High-Order Vorticity Confinement Schemes

Ilias Petropoulos[1], Michel Costes[1] and Paola Cinnella[2]

[1] ONERA, The French Aerospace Lab, 8 rue des Vertugadins, 92190 Meudon, France
[2] DynFluid Laboratory, Arts et Métiers ParisTech, 151 Bd. de l'Hôpital, 75013 Paris, France
Corresponding author: ilias.petropoulos@onera.fr

Abstract: High-order extensions of the Vorticity Confinement (VC) method are developed for the accurate computation of vortical flows, following the VC2 conservative formulation of Steinhoff. The original VC method is extended to 3rd and 5th-order of accuracy while the derivation procedure can be repeated to obtain even higher orders. The purpose of the study is to develop a VC formulation that maintains the vorticity preserving capability of the original 1st-order method and can be applied in high-order computations without compromising the global order of accuracy of the numerical scheme. Spectral analysis shows that the new method improves both the dispersive and dissipative properties of the baseline scheme whereas the increased precision of the new VC scheme and its increased compatibility with high-order methods is validated through numerical tests.

Keywords: Vortex Flows, Computational Fluid Dynamics, High-Order Schemes, Numerical Methods, Vorticity Confinement.

1 Introduction

Standard CFD methods have followed a course of steady improvement over the past decades and are adequate for modelling a large number of applications, but the accurate computation of vortical flows remains a challenge. The numerical schemes used in the solution of the flow equations need to be dissipative to ensure stability thus resulting in fast spreading and diffusion of vortex structures in computations. This weakness concerns both research and industry as the accurate advection of vortices is important in a broad spectrum of computational fluid dynamics applications such as wakes, separated flows and turbulence.

Lagrangian methods allow for a perfect preservation of vortices, but are usually inviscid and incompressible [1, 2]. Also, they often require special treatment for different applications and can have difficulties in computing complex flow states (e.g. vortex merging). Such characterics are hindering for the industry so these methods are rarely applied out of research for advanced aeronautics computations.

The formulation of Eulerian methods on the other hand is more robust and for this reason they are widely adopted. To treat the problem of vortex dissipation, the majority of the CFD community usually resorts to the use of finer meshes or automatic mesh adaptation methods [3, 4, 5] to increase the number of cells in the vicinity of vortical regions. However, there are drawbacks such as the significant increase of complexity and computational cost. Alternative hybrid methods to minimize the dissipation of vorticity can be constructed through domain decomposition by the coupling of structured-unstructured Eulerian [6, 7] or Eulerian-Lagrangian solvers [8, 9]. Such methods can combine the benefits of the different approaches in each region but are not always straightforward.

Another possibility is the use of high-order methods in the discretization of the fluid dynamics equations [10, 11, 12], which result in improved wave propagation properties. In the well-established Finite Volume method, the implementation of high-order flux derivatives is not simple, especially for non-Cartesian grids. Additionally, high-order methods are more expensive than standard methods and the dissipation of vortices still cannot be completely corrected. Furthermore, numerical schemes can be constructed specifically for

vorticity preservation [13, 14, 15]. However, the implementation of numerical schemes in a solver can be complicated and poses restrictions, so a more generic alternative method for vorticity preservation remains interesting.

Such an alternative is the Vorticity Confinement (VC) method proposed by J. Steinhoff [16, 17, 18], designed to capture small-scale features directly on the computational grid. In the present paper, we are working with the second (VC2) formulation [19, 20] of the method to ensure discrete momentum conservation. The capability of VC to preserve vorticity has been verified by extensive application in the aeronautics field over the past two decades. However, the original method remains 1st-order accurate and vortex structures are rapidly dominated by the VC source term. This effect is more important when a higher-order baseline scheme is used, where the lower-order term deteriorates the overall accuracy in vortical flow regions.

Due to the growth of high-order methods in both research and industrial applications [21], the construction of a Vorticity Confinement method that is appropriate for high-order computations shows great interest. Even more so, since in the vast majority of cases VC can be applied independently of the choice of the underlying numerical scheme and is not restricted to a specific formulation. High-order extensions of VC were analyzed for the linear advection equation [22], showing that the asymptotic solution over long distances is the same for all orders of accuracy, albeit at a lower convergence rate for higher orders. The slower convergence rate is in accordance with the lower numerical error that is associated with higher-order schemes, indicating a sound basis for an extension to the Euler/Navier-Stokes equations. First results on the Euler equations were presented for helicopter applications [23] while the complete method and its consistency with high-order flux discretizations have been thoroughly validated [24].

This paper consists of the following parts. Section 2 explains the VC formulation and the higher-order extension methodology for the linear advection case and the Euler/RANS equations. Section 3 presents a spectral analysis of the VC schemes, comparing analytical theory with a quasi-linear numerical method. In Section 4, a grid convergence study is performed to validate the order of accuracy and the developed schemes are applied in the advection of a 2D isentropic vortex over very long distances. Finally, the consistency of the VC schemes with complex flow dynamics are evaluated in the computation of the viscous Taylor-Green Vortex and the results are discussed in Section 5.

2 Description of the schemes

2.1 Linear transport equation

In the scalar case of the linear transport equation

$$u_t + au_x = 0 \quad with\ a > 0 \tag{1}$$

the VC method will be simply referred to as "confinement" since the transported variable does not specifically correspond to vorticity. The idea of confinement is to include an additional negative dissipation term to the existing space discretization in order to balance the dissipation of the numerical scheme. Considering a semi-discrete (continuous in time, discrete in space) approximation of the linear transport equation with confinement on a uniform grid with spacing h ($x_j = jh$, $j \in \mathbb{Z}$), the equation takes the generic form:

$$u_t + \mathcal{R}(u) + \varepsilon\,\mathcal{R}_C(\tilde{h}(u)) = 0 \tag{2}$$

where $\mathcal{R}, \mathcal{R}_C$ are space discretization operators and $\tilde{h}$ represents the harmonic mean of the transported variable between two neighboring points:

$$\tilde{h}(\bullet)_j = \begin{cases} \frac{2(\bullet)_j(\bullet)_{j-1}}{(\bullet)_j+(\bullet)_{j-1}} & ,if \quad (\bullet)_j(\bullet)_{j-1} > 0 \\ 0 & ,otherwise \end{cases} \tag{3}$$

The confinement term is the last term in Eq. (2). The operator $\mathcal{R}(u)$ represents the space discretization of the baseline scheme without confinement. The operator $\mathcal{R}_C(\tilde{h}(u))$ of the confinement term represents a space discretization for the harmonic mean of the transported variable between the neighboring cells for each stencil point, instead of the variable itself. The computational stencil of $\mathcal{R}_C(\tilde{h}(u))$ is again dependent

2

on the choice of the baseline scheme. The term is then multiplied by ε, which is a real constant called the confinement parameter.

In previous studies confinement was studied mostly on high-order extensions of the Lax-Wendroff and Warming-Beam schemes. In both of these cases an analysis of the space discretization is not straightforward due to coupling of the space and time terms. For this reason the present study focuses on a decoupled family of schemes, based on high-order centered space discretizations. Using the discretization operators $\delta(\bullet)_{j+\frac{1}{2}} := (\bullet)_{j+1} - (\bullet)_j$ and $\mu(\bullet)_{j+\frac{1}{2}} := \frac{1}{2}((\bullet)_{j+1} + (\bullet)_j)$ on a Cartesian mesh, the first and second derivatives can be approximated at 8th-order of accuracy on a 9-point stencil as [25, 26]:

$$
\begin{aligned}
(\bullet)^{(1)} &= \frac{1}{h}\delta\mu\left(I - \frac{1}{6}\delta^2 + \frac{1}{30}\delta^4 - \frac{1}{140}\delta^6\right)(\bullet) + O(h^8) \\
(\bullet)^{(2)} &= \frac{1}{h^2}\delta^2\left(I - \frac{1}{12}\delta^2 + \frac{1}{90}\delta^4 - \frac{1}{560}\delta^6\right)(\bullet) + O(h^8)
\end{aligned}
\tag{4}
$$

with I being the identity operator. The 6th, 4th and 2nd-order approximations can be obtained by recursively suppressing the δ^6, δ^4 and δ^2 terms. The discretization of the first derivative $(\bullet)^{(1)}$ in Eq. (4) is purely dispersive, so explicit artificial viscosity terms must be added for stability. Both artificial viscosity and the confinement term are based on higher-order differences of the second derivative of Eq. (4). Using the above approximations, a pth- (odd) order semi-discrete approximation of the linear transport equation (1) can be written as a sum of space discretization, artificial viscosity and the confinement term as:

$$
\frac{\partial u}{\partial t} + \frac{a}{h}\delta\mu\left(\sum_{l=0}^{(p-1)/2} b_l\delta^{2l}\right)u - \frac{a}{h}k_p\delta^2\left(\delta^{p-1}\right)u + \frac{a}{h}\varepsilon\delta^2\left(\delta^{p-1}\right)\tilde{h}(u) = 0
\tag{5}
$$

These baseline discretizations (without confinement) correspond to the DNC (Directional-Non-Compact) family of schemes derived by Lerat and Corre in [25] which are related to the MUSCL schemes of Van Leer based on Flux-Extrapolation without limiters (FE-MUSCL). The artificial viscosity coefficient k_p of Eq. (5) is always equal to the half of the coefficient of the higher-order term from the non-dissipative part of the scheme ($k_p = b_{(p-1)/2}/2$) providing dissipation equivalent to a non-compact upwind scheme [25].

The scheme of Eq. (5) will be referred to as the pth-order FE-MUSCL scheme with Confinement (FE-MUSCLp-C). By suppressing the last term, the baseline p^{th}-order FE-MUSCL scheme (FE-MUSCLp) is obtained.

2.2 Euler/RANS equations

Considering the original 1st-order VC2 formulation of Steinhoff, the VC term is added in the momentum equation as a source term. The conservative differential form of the momentum conservation equation can then be written:

$$
\frac{\partial \rho\vec{v}}{\partial t} + \vec{\nabla}\cdot\left(\rho\vec{v}\otimes\vec{v} + p\bar{\bar{I}} - \bar{\bar{\tau}}\right) = \rho\vec{f}
\tag{6}
$$

with the Vorticity Confinement term:

$$
\vec{f} = -\vec{\nabla}\times(\mu\vec{\omega} - \varepsilon\vec{w})
\tag{7}
$$

The first part is an artificial dissipation term with coefficient μ aligned with the vorticity vector $\vec{\omega} = \vec{\nabla}\times\vec{v}$. The second part is the negative dissipation confinement term with coefficient ε. This part is based on a vector $\vec{w}$ with magnitude equal to the harmonic mean of vorticity around the neighboring cells and aligned with vorticity as:

$$
\vec{w} = \frac{\vec{\omega}}{\|\vec{\omega}\|}\tilde{h}(\omega_j) = \frac{\vec{\omega}}{\|\vec{\omega}\|}N\left(\sum_{j=1}^{N}\|\vec{\omega_j}\|^{-1}\right)^{-1}
\tag{8}
$$

The introduction of a dissipation term in the VC formulation of Eq. (7) may appear counterintuitive, but is used in order to include explicit artificial dissipation in the order of the VC term that is explicitly applied in vortical regions and is independent of the dissipation of the numerical scheme.

3

The analogy of Eq. (6) with the confinement formulation in the case of the linear transport equation can be revealed by taking the curl of the momentum equation to derive the vorticity transport equation. By dividing with density we can obtain the specific vorticity transport equation, which in the case of a 2D isolated vortex in inviscid flow reduces to:

$$\frac{\partial(\vec{\omega}/\rho)}{\partial t} + \vec{v} \cdot \vec{\nabla}(\vec{\omega}/\rho) - \frac{1}{\rho}\vec{\nabla}^2\left(\mu\vec{\omega} - \varepsilon\vec{\mathrm{w}}\right) = 0 \tag{9}$$

$$or \quad \frac{\partial(\omega/\rho)}{\partial t} + \vec{v} \cdot \vec{\nabla}(\omega/\rho) - \frac{1}{\rho}\vec{\nabla}^2\left(\mu\omega - \varepsilon\tilde{h}(\omega_j)\right) = 0 \tag{10}$$

Furthermore, it has been shown that by ignoring the baseline scheme's dissipation, the asymptotic solutions of Eq. (10) are driven by the VC term and depend on the mesh size for given values of the confinement parameters, similarly to what is known for the asymptotic solutions of confinement for the linear transport equation [24].

By analogy with the δ operator in the linear scalar case, the curl operator can be recursively applied on the VC term of Eq. (7) to increase the order of differencing. By introducing the vector $\vec{\alpha} = -(\mu\vec{\omega} - \varepsilon\vec{\mathrm{w}})$ to simplify the equations and applying the curl operator twice on $\vec{f}$, we can introduce the equivalent of a δ^4 difference and obtain:

$$\vec{\nabla} \times \vec{f} = \vec{\nabla} \times \vec{\nabla} \times \vec{\alpha} = \vec{\nabla}\left(\vec{\nabla} \cdot \vec{\alpha}\right) - \vec{\nabla}^2\vec{\alpha}$$
$$\vec{f_3} = \vec{\nabla} \times \vec{\nabla} \times \vec{f} = -\vec{\nabla} \times \left(\vec{\nabla}^2\vec{\alpha}\right) = \vec{\nabla} \times \left(\vec{\nabla}^2\left(\mu\vec{\omega} - \varepsilon\vec{\mathrm{w}}\right)\right) \tag{11}$$

A 4th-difference extension of VC can therefore be obtained by taking the Laplacian of the original term. It is important to note that the Laplacian is rotationally invariant similarly to the idea of the original VC method as proposed by Steinhoff. Furthermore, the alternate sign of higher-order derivatives is naturally introduced by the recursive applications of the curl operator. Since the higher difference alone does not suffice, the use of undivided differences in the computation of the Laplacian will ensure consistency with the original partial differential equation and provide increased order of accuracy. Similarly, the 5th-order VC term is obtained by taking the bi-Laplacian of the VC term of Eq. (7). Note also that both the original VC and the higher-order extensions are independent from the choice of space discretization or time integration scheme.

The analogy of Eq. (11) with Eq. (7), can be investigated by taking the curl of the developed scheme, which corresponds to the vorticity transport equation (10). In the case of an isolated 2D vortex in inviscid flow:

$$\begin{aligned} \vec{\nabla} \times \vec{f_3} \quad &= -\vec{\nabla} \times \left(\vec{\nabla} \times \vec{\nabla}^2\vec{\alpha}\right) \\ &= -\vec{\nabla}\vec{\nabla} \cdot \left(\vec{\nabla}^2\vec{\alpha}\right) + \vec{\nabla}^2\left(\vec{\nabla}^2\vec{\alpha}\right) \\ &= -\vec{\nabla}\vec{\nabla} \cdot \left(\vec{\nabla}^2\left(\mu\vec{\omega} - \varepsilon\vec{\mathrm{w}}\right)\right) + \vec{\nabla}^2\left(\vec{\nabla}^2\left(\mu\vec{\omega} - \varepsilon\vec{\mathrm{w}}\right)\right) \\ &= -\vec{\nabla}\vec{\nabla} \cdot \left(\vec{\nabla}\left(\vec{\nabla} \cdot \mu\vec{\omega} - \vec{\nabla} \cdot \varepsilon\vec{\mathrm{w}}\right) - \vec{\nabla} \times \vec{\nabla} \times \left(\mu\vec{\omega} - \varepsilon\vec{\mathrm{w}}\right)\right) + \vec{\nabla}^2\left(\vec{\nabla}^2\left(\mu\vec{\omega} - \varepsilon\vec{\mathrm{w}}\right)\right) \\ &= \vec{\nabla}^2\left(\vec{\nabla}^2\left(\mu\vec{\omega} - \varepsilon\vec{\mathrm{w}}\right)\right) \tag{12} \end{aligned}$$

since vorticity is perpendicular to the gradient of the harmonic mean of vorticity modulus for a 2D vortex. The new term is therefore analogous to the VC term of Eq. (9), expressed as the sum of a dissipation and a confinement term.

The confinement parameters are always multiplied by the mesh size for consistency. In the presentation of results it has been chosen to express the confinement parameters as ε, μ/ε as the first is a measure of the intensity of the confinement part and the second represents the ratio between explicit artificial dissipation and confinement within the VC term. The flow regions, where VC is applied, are selected based on a cut-off value of the Q-criterion.

4

3 Spectral analysis for the scalar case

The dispersive and dissipative properties of confinement schemes are evaluated for the scalar formulation of confinement presented in Subsection 2.1. Spectral analysis is performed analytically based on linear theory and using a quasi-linear numerical method.

3.1 Linear theory

A spectral analysis of confinement schemes is not straightforward because the confinement term of Eq. (2) is intrinsically non-linear. However, confinement schemes can be linearized using exponent functions, which behave like eigenfunctions for the harmonic mean on a uniform grid. This property becomes apparent when we consider a single harmonic $u_j^n = \hat{u}^n e^{ij\xi}$ with assigned reduced wavenumber $\xi = kh$ for the linear transport equation. Then, for a uniform grid with spacing h ($x_j = jh$, $j \in \mathbb{Z}$) and a time step Δt ($t = n\Delta t$, $n \in \mathbb{Z}$):

$$\tilde{h}(u)_j = 2\left((u_j)^{-1} + (u_{j-1})^{-1}\right)^{-1} = 2\left(1 + e^{i\xi}\right)^{-1} u_j^n \tag{13}$$

where the factor of u_j in the above expression is independent of the position on the computational grid. Considering a single harmonic and taking advantage of Eq. (13), a semi-discrete approximation can be written in the form of the exact solution of Eq. (1), which is a travelling wave:

$$u_j(t) = u_0 e^{ij\xi} e^{-i(at/h)\xi} \tag{14}$$

If η are the coefficients of the expanded centered difference operators of Eq. (5), it is:

$$\delta\mu\left(\delta^m(\bullet)_j\right) = \sum_{q=1}^{1+(m/2)} \eta_q(\bullet)_{j+q} - \eta_q(\bullet)_{j-q} \tag{15}$$

Then, after some algebraic developments, the modified wavenumber of the pth-(odd) order FE-MUSCL space discretization of Eq. (5) with confinement (FE-MUSCLp-C) can be expressed with the recurrence relation:

$$\xi_p^* = \sum_{l=0}^{(p-1)/2} b_l \left(\sum_{q=1}^{l+1} \eta_q \sin(q\xi)\right) + i\, 2^{(p+1)/2}(-1)^{(p+3)/2} k_p \left(\cos\xi - 1\right)^{(p+1)/2}$$

$$+ 2^{(p+1)/2}(-1)^{(p+1)/2}\,\varepsilon\,\sin\xi\,\frac{(\cos\xi - 1)^{(p+1)/2}}{\cos\xi + 1} + i\, 2^{(p+1)/2}(-1)^{(p+1)/2}\,\varepsilon\,(\cos\xi - 1)^{(p+1)/2} \tag{16}$$

where the first term corresponds to the centered space discretization, the second to the explicit artificial viscosity and the last two correspond to confinement. By suppressing the terms associated with ε in Eq. (16), the expression for the pth-order baseline FE-MUSCL scheme is obtained.

For the exact solution of the linear transport equation (Eq. (14)) it is $\xi^* = \xi$, therefore $|Re(\xi^*) - \xi|/\pi$ can be used as a measure of dispersion or phase approximation error and $Im(\xi^*)$ can be used as a measure of dissipation error of the schemes (5) compared to the exact solution. Note that in Eq. (16), dissipation derives only from the artificial dissipation and confinement terms.

Fig. 1 compares the dispersive properties of FE-MUSCL-C confinement schemes with the corresponding baseline FE-MUSCL schemes up to 7th-order of accuracy. The confinement parameter is $\varepsilon = 1.14\,k_p$ for all cases. As illustrated in the analytical expression of Eq. (16), even though confinement is originally based on an even difference, its non-linear character introduces modifications both in the dispersive and dissipative properties of the scheme. Fig. 1 shows that confinement decreases the phase approximation error of FE-MUSCL schemes at least up to the grid resolvability limit $\xi = \pi/2$ for all orders. On the other hand, Eq. (16) shows that $Im(\xi^*) > 0$ (i.e. instability) for confinement schemes since $\varepsilon > k_p$ to ensure that the numerical scheme is globally anti-dissipative. This however is not in agreement with extensive numerical experiments, which have verified the stability of confinement schemes [22, 27, 28]. The inconsistency of analytical theory is explained from the linearization considered in Eq. (13), which permits the application of linear stability theory, but can in no case express the complete non-linearity of the confinement term.
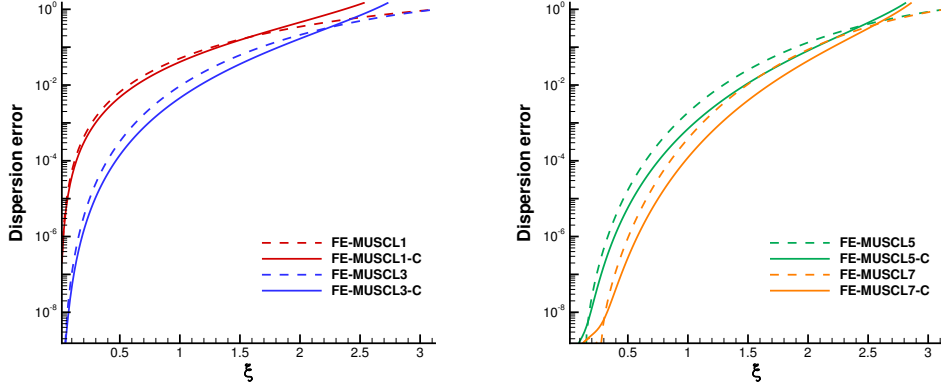
Figure 1: Dispersion error of FE-MUSCL schemes up to 7th-order with and without confinement for $\varepsilon = 1.14\,k_p$

3.2 Numerical evaluation

Given the inability of analytical theory to represent the non-linear confinement schemes, the aim of this section is to evaluate their spectral properties using a numerical approach proposed by Pirozzoli [29] for the study of non-linear shock capturing schemes. This method was shown to produce an improved prediction compared to conventional analyses, providing results in general agreement with observations on the properties of these schemes after their application in numerical experiments.

Again, we consider sinusoidal monochromatic initial conditions with assigned reduced wavenumber ξ for Eq. (1) on a uniform grid with spacing h ($x_j = jh$, $j \in \mathbb{Z}$):

$$u_j^0 = \hat{u}^0 e^{ij\xi} \tag{17}$$

For all wavenumbers in the range $[0 - \pi]$ that result in periodic initial conditions of the type (17) on the finite computational grid, the numerical scheme is used to advance the initial signal to a very small time τ. The time τ must be sufficiently small in order to exclude time integration error and in turn ensure that the initial conditions remain monochromatic at the end of the computation.

The modified wavenumber can then be derived from the Discrete Fourier Transform of the initial and computed signal for each supported wavenumber ξ in the range $[0 - \pi]$:

$$\xi^*(\xi) = -\frac{1}{i\sigma} log \left(\frac{\hat{u}(\xi;\tau)}{\hat{u}(\xi;0)} \right) \tag{18}$$

The numerical method is first validated through comparison with analytical results of Subsection 3.1. Fig. 2 shows that the numerical method is in excellent agreement with analytical results for linear schemes, for which linear theory is exact, in the complete wavenumber spectrum. Similar results were obtained for the confinement schemes based on high-order extensions of the Lax-Wendroff scheme of [22], since the time-coupled terms of these schemes disappear for a very small value of the CFL number.

It can be seen in Fig. 2 that numerical method results for confinement schemes are not smooth everywhere in the wavenumber space. Specifically, "spikes" can be observed for $\xi \in \mathcal{S} = \{\pi/2,\, 3\pi/4,\, 4\pi/5,\, 9\pi/10\}$, wavenumbers equal or greater than the grid resolvability limit $\pi/2$ posed by the Nyquist-Shannon theorem. At these points, confinement appears to have no effect and the result matches exactly the curves of the baseline FE-MUSCL scheme. This behaviour is related to the harmonic mean function of Eq. (3), which is only defined for numbers of the same sign and therefore is set to zero otherwise. For frequencies of the set $\mathcal{S}$, the initial condition is such that $h(u_j, u_{j-1}) = 0 \quad \forall j \in \{0, 1, ..., N\}$ and the total contribution of confinement is exactly zero. This weakness of confinement however refers to single harmonics and was not observed in general problems, since frequencies higher than $\pi/2$ are under-resolved and should in any case
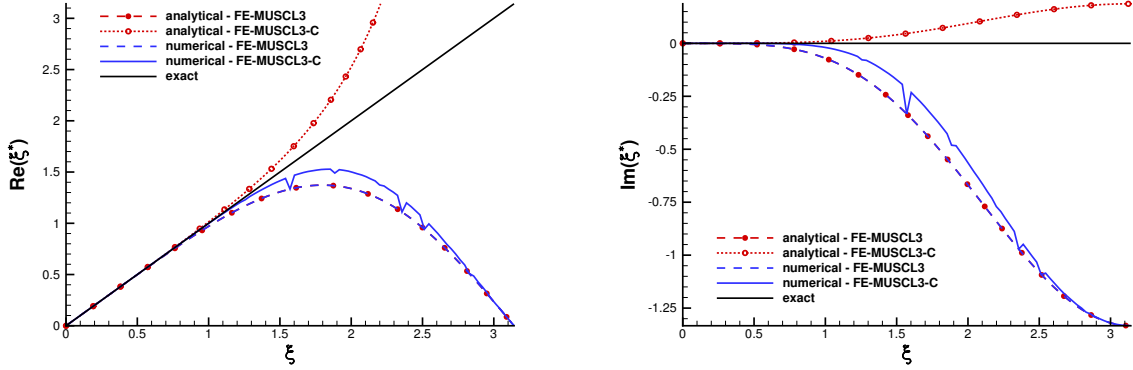
Figure 2: Comparison of the numerical spectral analysis method with linear theory. Baseline FE-MUSCL3 scheme and with confinement ($\varepsilon = 1.14\,k_p$).

be damped by filters or the numerical scheme's inherent dissipation.

Results of the numerical method are shown in Fig. 3 for high-order FE-MUSCL schemes with and without confinement up to 7th-order of accuracy. As expected, higher-order schemes provide a good approximation of the exact solution for a longer range of wavenumbers. Fig. 3 also shows that the developed confinement schemes are stable and have improved dispersive and dissipative properties compared to their linear counterparts with the exception of wavenumbers $\xi \in \mathcal{S}$ where their properties are reduced to those of the baseline scheme. Confinement can also achieve the preservation of waves over arbitrarily long distances [22, 24], a non-linear property which is not taken in account by the present analysis but cannot be achieved even for high-order baseline schemes. The improvement in terms of dispersion is not obvious, since the confinement term of Eq. (5) is originally based on a dissipative operator, but is associated to the non-linear properties of the term. Additionally, confinement acts in a rate that matches the order of the baseline scheme since its effect is smaller as the order increases, or equivalently when numerical error is reduced. Finally, the negative dissipation introduced by confinement does not affect the damping of the shortest wavelength $\xi = \pi$, which is associated to grid-to-grid oscillations.
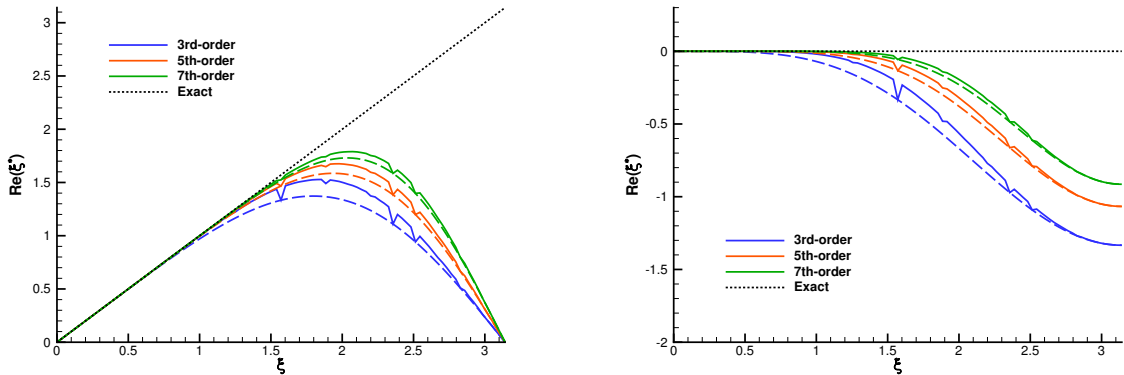

Figure 3: Spectral properties of FE-MUSCL schemes up to 7th-order. Baseline schemes (dashed lines) and with confinement (solid lines), $\varepsilon = 1.14\,k_p$.

The accuracy of numerical schemes can be quantified by comparing their resolvability limit in the wavenumber space, or equivalently by computing the maximum wavenumber ξ_n for which the scheme approximates the exact solution under a defined error threshold E. In turn, this reduced wavenumber is equivalent

to a minimum number of grid points per wavelength λ_n/h to ensure the accurate computation of the advection. Tables 1-2 show the effect of confinement on the resolvability limit of FE-MUSCL schemes due to dispersion and due to dissipation. The FE-MUSCL schemes of Eq. (5) are odd-order accurate and therefore have a leading truncation error term of dissipative nature, the accuracy limit being in turn defined by their dissipation error, rather than dispersion. Confinement is shown to achieve a considerable improvement of this limit due to dissipation, halving the minimum number of points per wavelength for the FE-MUSCL3 scheme and extending the well-resolved wavenumber range even for the more precise FE-MUSCL5/FE-MUSCL7. Furthermore, confinement is shown to improve phase errors by an amount comparable to the improvement in terms of dissipation, even though the method had not been designed for this purpose.

Table 1: Resolvability limit due to dispersion for FE-MUSCL schemes ($E = 10^{-3}$)

	baseline		confinement	
	ξ_n	λ_n/h	ξ_n	λ_n/h
FE-MUSCL3	0.471	13.33	0.974	6.45
FE-MUSCL5	0.754	8.33	1.005	6.25
FE-MUSCL7	0.974	6.45	1.131	5.56

Table 2: Resolvability limit due to dissipation for FE-MUSCL schemes ($E = 10^{-3}$)

	baseline		confinement	
	ξ_n	λ_n/h	ξ_n	λ_n/h
FE-MUSCL3	0.314	20.00	0.660	9.52
FE-MUSCL5	0.628	10.00	0.848	7.41
FE-MUSCL7	0.880	7.14	1.037	6.06

It can be argued that, having a higher cut-off wavenumber both in terms of dispersion and dissipation, the FE-MUSCL3-C scheme with confinement is a preferable choice over the baseline FE-MUSCL5 scheme. This is true for $\xi < \xi_n$, but not representative of the complete wavenumber range, where the FE-MUSCL5 shows overall superior properties (Fig. 3). Furthermore, spectral analysis represents only wave propagation properties and not the improved approximation of the convective derivative provided by the FE-MUSCL5 scheme. Confinement is not equivalent to a correction of the leading truncation error term but represents a conservative correction to the baseline scheme allowing the accurate calculation of wave advection over arbitrarily long distances. This makes confinement an interesting approach for diffusion-dominated problems, but it is not capable of preserving structures not captured by the baseline scheme.

4 Numerical results

The Vorticity Confinement schemes presented in Subsection 2.2 were integrated into the DynHoLab Finite Volume solver of DynFluid laboratory [30] up to 5th-order of accuracy. In the following these schemes are applied in the calculation of compressible vortical flows and evaluated based on their numerical error, vorticity-preserving capabilities and non-linear dynamics.

4.1 Grid convergence

The first validation case is a grid convergence study of a static 2D vortex, using the isentropic vortex model of Yee et al. [31]. The isentropic vortex is initialized on a flow at rest and its evolution is computed based on the Euler equations, meaning that any spreading and diffusion are attributed to the dissipation of the numerical scheme. The velocity and vorticity vectors in Crocco's form of Euler's momentum equation are perpendicular, meaning that the flow cannot remain fully isentropic. However, the entropy gradient remains small, thus allowing an analysis with a reasonable approximation of the isentropic case [24].

Computations are performed on a square Cartesian mesh $-5 < x < 5$, $-5 < y < 5$ and the vortex is initialized at the center of the computational domain at $x = y = 0$. Different meshes of varying density were considered, ranging from $\Delta x = 0.4$ (625 cells) for the coarsest mesh to $\Delta x = 0.025$ (160000 cells) for the finest mesh with Δx being halved between two successive cases. Periodicity conditions were imposed on each side of the computational domain. Computations were run from $t = 0$ to $t = 1$ using a small fixed ratio of $\frac{\Delta t}{\Delta x} = 2 \cdot 10^{-4}$ for all cases, to minimize any error introduced by time integration. Space discretization is performed using FE-MUSCL schemes [25] of order ranging from 1st to 5th and time integration is performed using a classical 4-step Runge-Kutta algorithm. For cases where VC is applied, the confinement parameters are set to $\mu/\varepsilon = 0.6$, $\varepsilon = 0.02$. Last, the cut-off value of the Q-criterion is set to 0.1 for all presented cases.
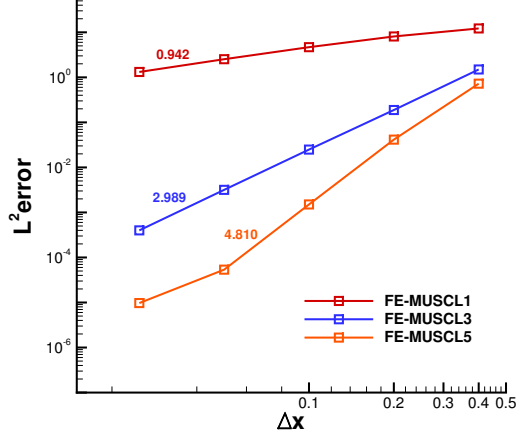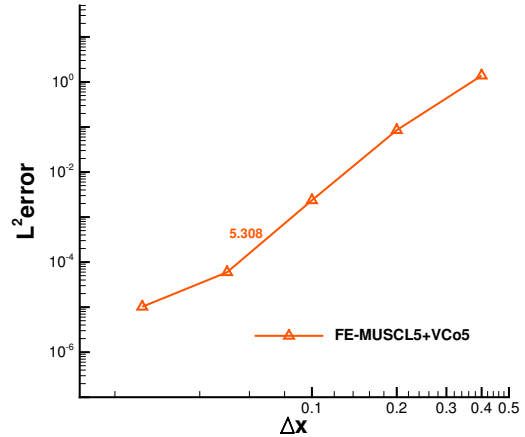

(a) Baseline FE-MUSCL schemes
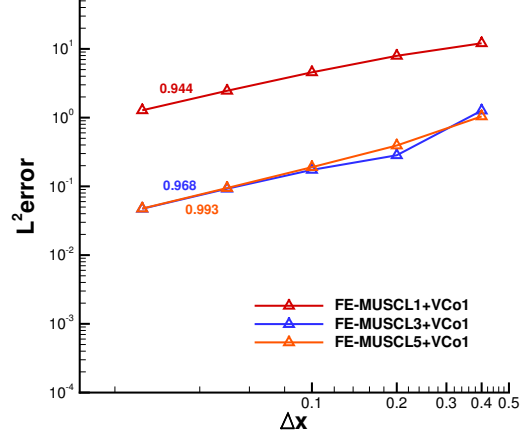
(b) FE-MUSCL and 1st-order VC
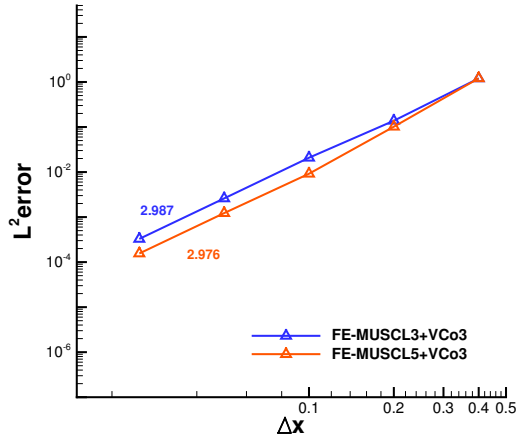
(c) FE-MUSCL and 3rd-order VC

(d) FE-MUSCL and 5th-order VC

Figure 4: Error convergence for FE-MUSCL schemes with and without VC.

The final solution is compared to the initial isentropic field and the L^2 norm of entropy error is computed based on the cell-averaged solution at cell centers:

$$L^2\,error = \left[\frac{\sum\limits_{i=1}^{n} |\bar{s}_i - \bar{s}_{i,exact}|^2 vol_i}{\sum\limits_{i=1}^{n} vol_i} \right]^{1/2} \tag{19}$$

Fig. 4(a) shows the L^2 norm of entropy error for FE-MUSCL schemes of 1st, 3rd and 5th-order of accuracy. The nominal convergence slope is correctly obtained, but a slope decrease can be observed for the 5th-order FE-MUSCL scheme for very fine grids. A similar behaviour has been observed in previous studies [24] for fine enough resolution and is probably due to the isentropic vortex not being an exact solution of the Euler equations, as is assumed during the error analysis.

Fig. 4(b) underlines the incompatibility of the original VC method with higher-order schemes, as the numerical error of the VC term dominates the solution, resulting in a 1st-order convergence slope regardless of the underlying scheme. Furthermore, Figs. 4(c) and 4(d) show that with the developed higher-order VC extensions, the nominal order of accuracy is recovered. The decrease in convergence slope is observed for the 5th-order FE-MUSCL scheme with 5th-order VC as for the baseline case.

4.2 Diagonal vortex advection

The FE-MUSCL schemes used in the present work, as well as the majority of numerical schemes in general, are directional, meaning that numerical error is increased when the grid is not aligned with the direction of advection. The second test case considers the advection of a 2D vortex in an inviscid uniform flow inclined by $45°$ with respect to the grid, so as to underline the effect of numerical error of both the baseline and the VC method.

The advection is studied on a square computational domain extending from $x = y = -15$ to $x = y = +15$. The nondimensional flow velocity components are $u = v = 1$ so that $U = \sqrt{2}$ in the diagonal direction and the fluid variables are $\gamma = 1.4$, $p_{inf} = 1/\gamma$, $\rho_{inf} = 1$. The isentropic vortex is initialized at $x_0 = y_0 = -10$ using the isentropic model of Yee et al. [31] as for the previous case. The problem is solved on a coarse 100×100 Cartesian grid with approximately 4 cells across the vortex core and periodicity conditions are imposed in each side of the domain. Time integration is performed with a 4-step explicit Runge-Kutta algorithm and a time step $\Delta t = 0.025$ for all cases, meaning an approximate $CFL \approx 0.083$. Note that a full advection is completed in time $T = 30$.

The case was studied using both 3rd- and 5th-order FE-MUSCL baseline schemes and the advection was computed over a distance of 30 and 300 passages across the computational domain respectively for each case. For the cases where VC was applied, the value of the confinement parameters is defined empirically depending on the numerical error of the baseline scheme, corresponding to stronger VC for a baseline scheme of lower order. The values, independently of the order of the VC term, were set to $\mu/\varepsilon = 0.2$, $\varepsilon = 0.16$ for FE-MUSCL3 and $\mu/\varepsilon = 0.4$, $\varepsilon = 0.02$ for FE-MUSCL5.

It should be noted that this case is not expected to display significant difference between VC schemes of different order. This is because the difference in the error convergence of high-order VC for such a coarse mesh ($\Delta x = 0.3$) is not significant with respect to the 1st-order one (see Figs. 4(a)-4(d)). The purpose of this study is therefore to demonstrate the vorticity preserving capability of all orders of VC at very coarse meshes. For more refined cases it is known that the negative dissipation of the 1st-order VC term does not decrease according to the order of the baseline scheme, resulting in a rapid amplification of the advected structure [24] and making the use of high-order VC mandatory.

Fig. 5 shows iso-density contours during the advection of the vortex for the 3rd-order FE-MUSCL case. The effect of dissipative error is severe for the baseline scheme leading to a complete diffusion of the vortex after 30 passages across the computational domain. The 1st-order VC method achieves a good preservation of vortex intensity, but introduces significant dispersion error along the vertical direction. The 3rd-order VC scheme has similar vorticity preserving capabilities with a more accurate trajectory prediction than the 1st-order one.

(a) Baseline FE-MUSCL3 scheme

(b) FE-MUSCL3 and 1st-order VC

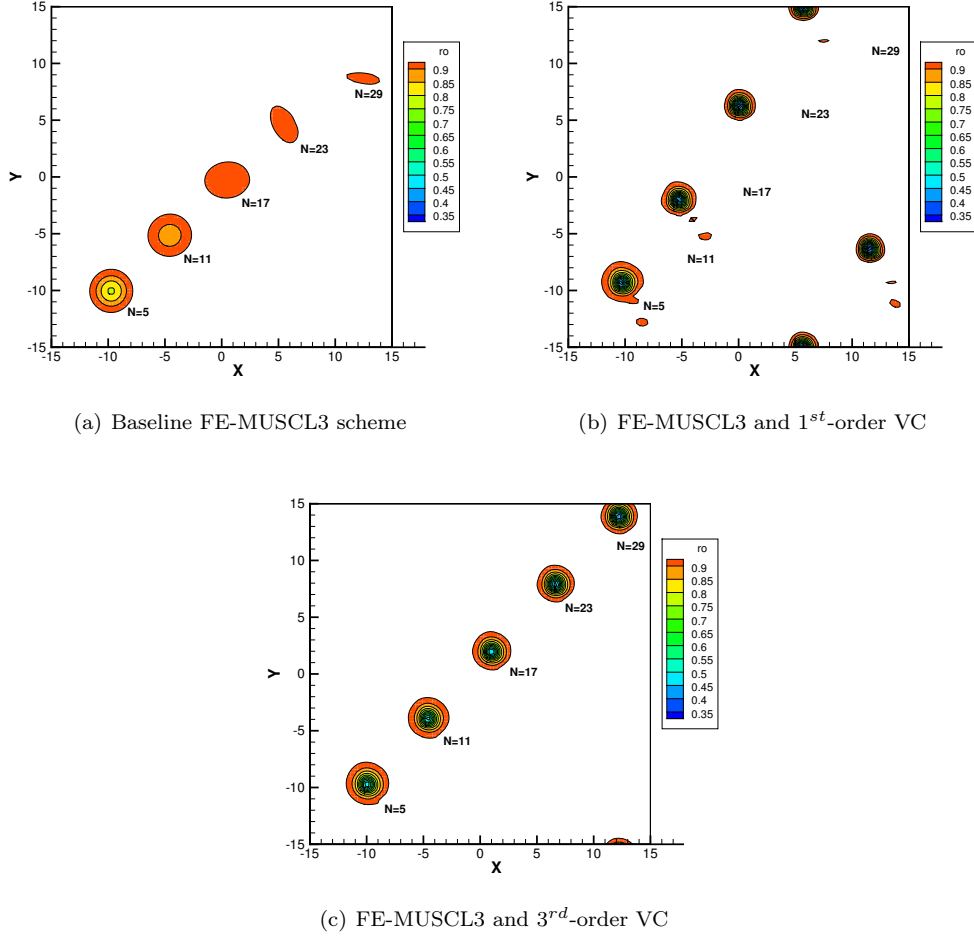(c) FE-MUSCL3 and 3rd-order VC

Figure 5: Iso-density contours during the diagonal vortex advection using the FE-MUSCL3 scheme. The approximate number of completed passages at each moment is indicated next to the corresponding contour.
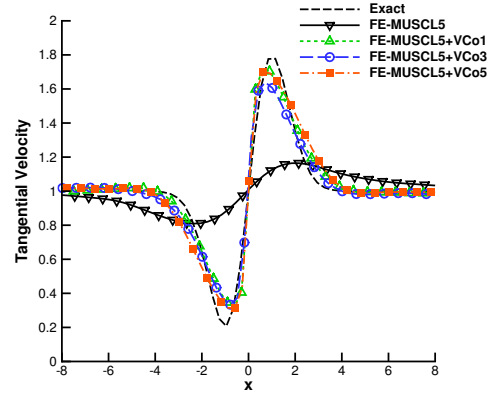
Horizontal extractions of tangential velocity profiles at the end of the computation are shown in Fig. 6 and are used as a measure of the schemes' vorticity preserving properties. All curves have been centered at $x = 0$ for the sake of comparison. Computed profiles show some spreading with respect to the exact solution, especially for FE-MUSCL3. However, VC clearly improves the vorticity preserving capabilities of both 3rd-order and 5th-order FE-MUSCL schemes and produces satisfactory results especially considering the coarse mesh resolution and the length of the computed distance.

The trajectory error with respect to the exact solution, which is the passive advection of the vortex along the diagonal, is shown in Fig. 7 as a measure of the schemes' phase approximation. For both FE-MUSCL3 and FE-MUSCL5 cases, the 1st-order VC term exhibits a significant dispersion error in the vertical direction since the early stages of the advection. High-order VC schemes show overall decreased error in vortex trajectory compared to the baseline one even though no clear conclusion can be made regarding the order of accuracy of VC in this case.

It is clear in this study that schemes with VC have significantly improved vorticity preservation properties compared to baseline ones for all orders of the VC term. On very coarse meshes, high-order VC is not significantly closer to the exact solution compared to the original 1st-order one, the difference appearing mostly in terms of dispersion error. However, for finer meshes, the use of VC of the same order as the baseline scheme is important to guarantee consistency in terms of convergence towards the exact solution and to ensure that VC acts at a rate that matches the numerical error of the baseline scheme.
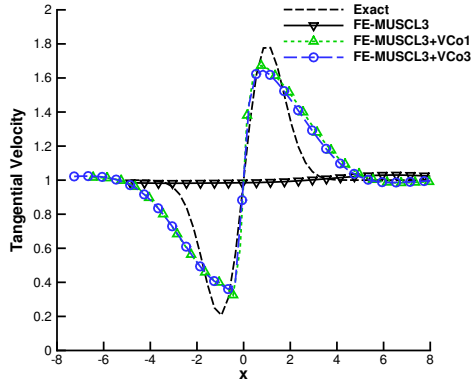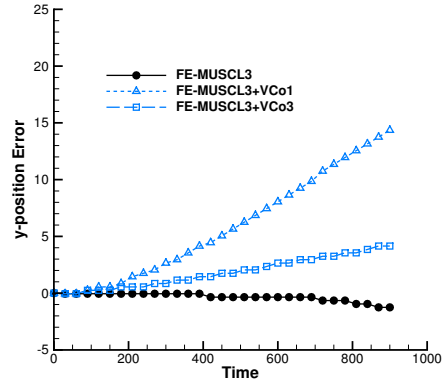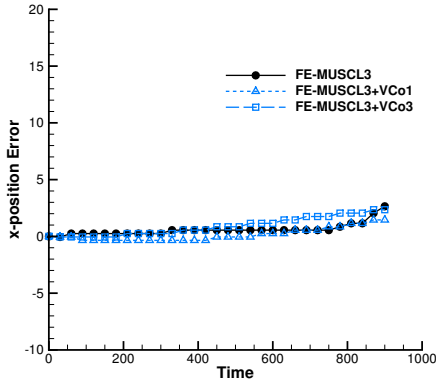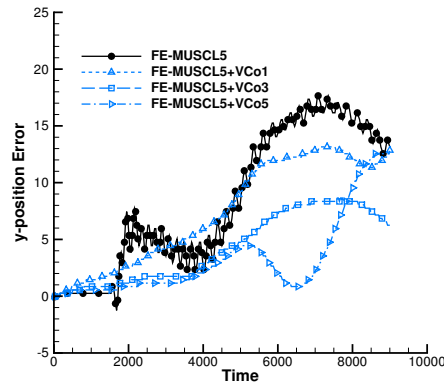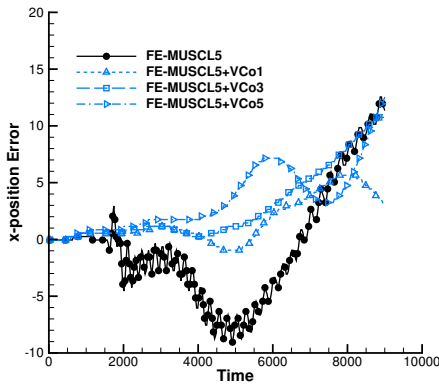
(a) FE-MUSCL3, profiles at $t = 900$ (b) FE-MUSCL5, profiles at $t = 9000$

Figure 6: Comparison of tangential velocity profiles at the end of the computation. FE-MUSCL schemes with and without VC.

(a) FE-MUSCL3

(b) FE-MUSCL5

Figure 7: Error in trajectory calculation for FE-MUSCL schemes and VC.

4.3   Viscous Taylor-Green Vortex

The final case is the study of the Taylor-Green Vortex (TGV) [32] at $Re = 1600$ which has been considered a benchmark test case for recent high-order CFD workshops [21] and high-precision numerical methods [33, 34]. The TGV flow is an unsteady problem with an analytical initial condition that consists of energy transfer from large to smaller scales through viscous, stretching and tilting mechanisms. For the viscous case, kinetic energy cascade occurs due to fluid viscosity and numerical dissipation as well as interaction and decay mechanisms that are characteristic of homogeneous turbulence.

It is therefore chosen as the last case to assess the robustness and performance of high-order Vorticity Confinement. The objective of this assessment is twofold. Having already proved the capabilities of VC to overcome numerical dissipation and allow the advection of vortical structures over long distances, the primary objective is the investigation of the effect of VC in the dynamics of a complex and multi-scale flow, representative of a broad range of Large Eddy Simulation (LES) applications. The secondary objective is the evaluation of the improvement introduced by VC in the prediction of the TGV flow, compared to baseline upwind FE-MUSCL schemes.

The compressible Navier-Stokes equations are solved on a cubic computational domain $[2\pi]^3$ on Cartesian meshes of varying density with a total number of cells 32^3, 64^3, 128^3, 256^3. Convective fluxes are discretized using the same FE-MUSCL schemes as for the previous studies [25]. Time integration is performed using an explicit 6-stage Runge-Kutta algorithm, formally accurate to 2nd-order, with optimized coefficients to ensure minimal dispersive and dissipative error [35]. The time step is set equal to $0.01/0.005/0.0025/0.00125$ for the coarser to the finer mesh respectively, so that the CFL number is kept constant for all cases. The VC term is always of the same order as the baseline scheme and the confinement parameters are $\mu/\varepsilon = 0.4$, $\varepsilon = 0.02$ as for the diagonal vortex advection case. Results are compared against the reference case of the International Workshop of High-Order CFD Methods, which is a converged DNS computation using a dealiased pseudo-spectral method on a 512^3 mesh.

Fig. 8 shows a grid convergence study for the baseline FE-MUSCL5 scheme. The dissipation rate (i.e. the time derivative of the integrated kinetic energy K over the computational domain) converges fast towards the DNS results, that are well matched already on the 256^3 mesh, except at the end of the turbulence decay phase. The evolution of integrated enstrophy E over the domain is more difficult to match, since it contains the accumulated error in the computation of conservative variables and velocity gradients over the computational domain. It is thus often used as a criterion for the convergence of results for the TGV flow. For an incompressible flow without numerical dissipation the kinetic energy dissipation rate is related to enstrophy via $-\frac{dK}{dt} = 2\frac{\mu}{\rho_0}E$.
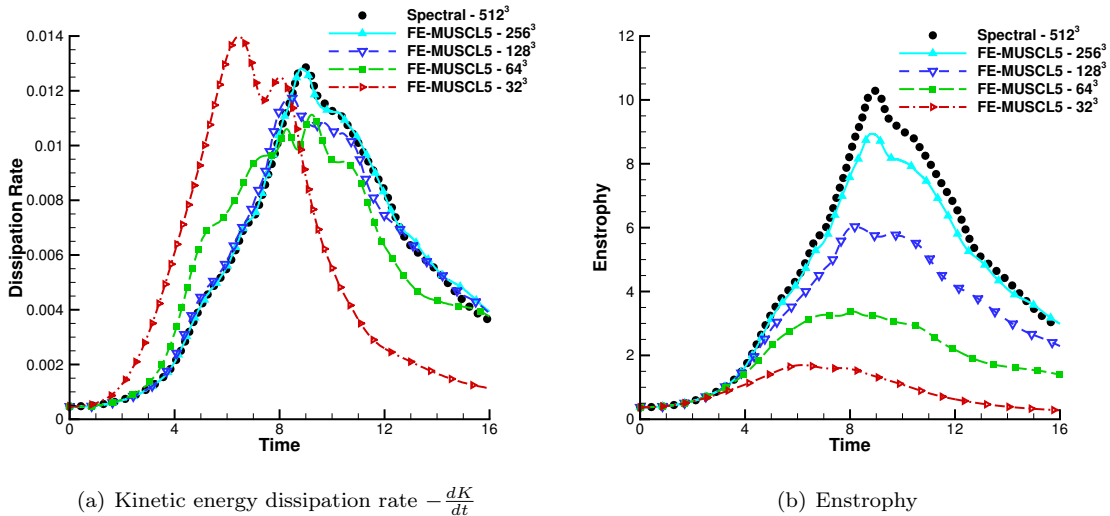

(a) Kinetic energy dissipation rate $-\frac{dK}{dt}$ (b) Enstrophy

Figure 8: Grid convergence for enstrophy and kinetic energy dissipation rate $-\frac{dK}{dt}$ using the 5th-order FE-MUSCL scheme.

The TGV problem is initially dominated by vortex stretching and tilting mechanisms, generating smaller and smaller vortical structures up to the time at which the dissipation rate peaks ($t \approx 9$). The flow then transitions to fully developed non-isotropic turbulence and finally decays due to the dissipation acting at the smaller scales (snapshots of the flow computed with VC are shown in Fig. 9).
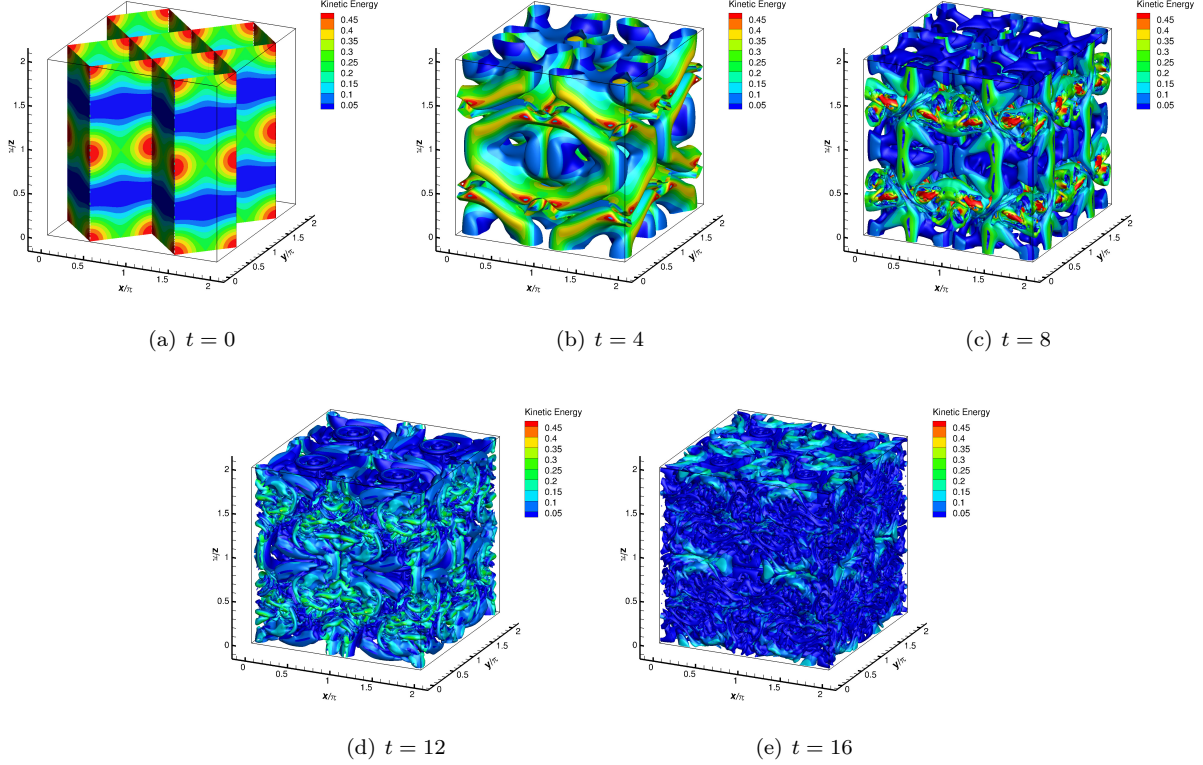

Figure 9: Iso-surface of $Q = 0$ colored by kinetic energy computed with FE-MUSCL5 and 5th-order Vorticity Confinement on the 256^3 mesh.

The left column of Fig. 10 shows the difference of the time evolution of the kinetic energy dissipation rate between the baseline case and the FE-MUSCL5 scheme with VC. For the 64^3 and 256^3 meshes, VC is consistent with the vorticity dynamics of the flow, reducing dissipation during the vortex stretching phase and later on increasing the dissipation peak since it improves the preservation of small structures that largely contribute to this dissipation. For the 128^3 case VC is constantly reducing dissipation, being in better agreement with the reference computation than the baseline FE-MUSCL5 scheme during the vortex stretching phase, but does not increase the dissipation peak. Furthermore, the effect of VC is smaller when the mesh is refined, or equivalently when numerical dissipation is reduced, displaying consistent behaviour with the baseline 5th-order scheme for the vortex stretching phase and up to the development of turbulence. Regarding this last stage, VC increases dissipation compared to the baseline scheme due to the improved preservation of eddies in the inertial range, even when the baseline case is quite well-converged towards the reference results.

The time evolution of enstrophy is shown in the right column of Fig. 10 for the same cases. Results are straightforward meaning that VC acts in vortical regions by introducing negative dissipation in the vorticity transport equation and therefore increases the integral value of enstrophy, in a sense accelerating the convergence towards the DNS solution. Compared to the time evolution of the dissipation rate, the effect of VC on enstrophy does not decrease with mesh refinement: this is a result of the improved resolution of vortical structures (i.e. a VC term that is better aligned with local vorticity and therefore more efficient) and does not represent an inconsistency with respect to the convergence order of the baseline discretization.
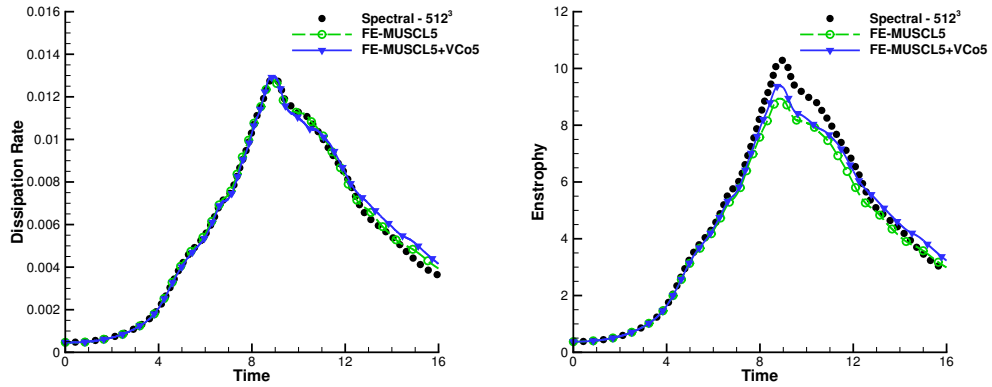
This is further demonstrated by the iso-contours of the dimensionless vorticity norm on a periodic face

14
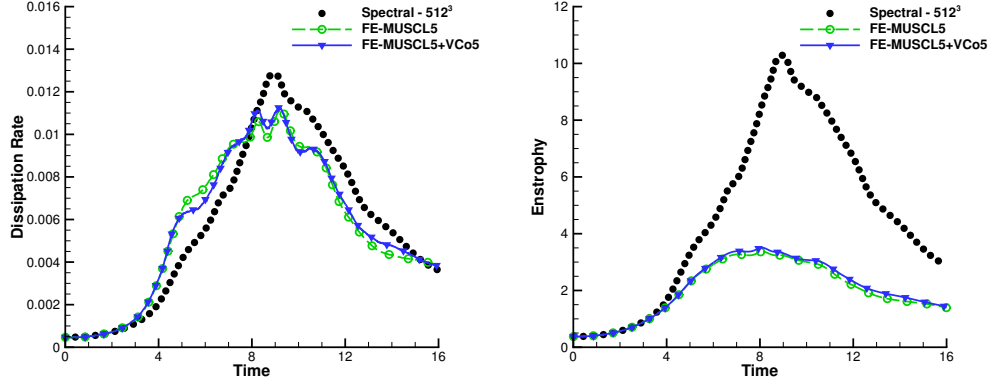
(a) 64^3 mesh
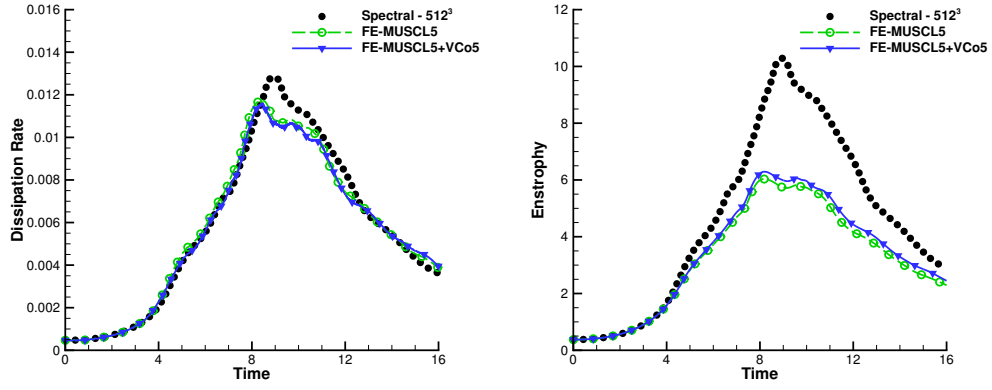
(b) 128^3 mesh

(c) 256^3 mesh

Figure 10: Effect of VC on the kinetic energy dissipation rate and the evolution of enstrophy for varying mesh density. FE-MUSCL5 and 5th-order Vorticity Confinement.

of the computational domain at $t = 8$, presented in Fig. 11. Results of the VC and baseline FE-MUSCL5 scheme are compared to the reference spectral results and provide a good approximation of the main flow structures. VC improves the preservation of vortices without introducing unphysical changes in the structure

15

(a) FE-MUSCL5 - 256^3 mesh   (b) FE-MUSCL5 + VCo5 - 256^3 mesh   (c) Spectral - 512^3 mesh
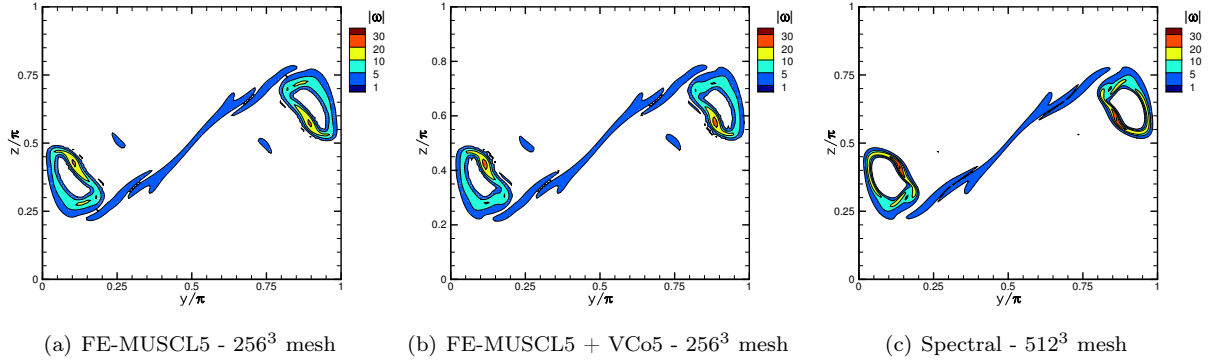
Figure 11: Iso-contours of the dimensionless vorticity norm $|\omega|$ on the periodic face $x/L = -\pi$ at nondimensional time $t = 8$.

shape.

This preliminary study shows that schemes with VC are consistent with the dynamics of the complex TGV flow without the need for a special treatment or a more sophisticated choice of confinement parameters compared to a simple isolated 2D vortex case. Furthermore, the developed VC schemes introduce an improvement to the baseline scheme over the vortex stretching phase where the treatment of large structures is involved. However, VC increases the life-span of vortices during the turbulence decay phase, eventually producing more dissipation at the smallest scales, a behaviour which will be further investigated in future studies.

5 Conclusions

This paper presents high-order extensions of Vorticity Confinement for the accurate calculation of compressible vortical flows. In the scalar advection case, a quasi-linear numerical spectral analysis shows that the developed non-linear schemes have improved dispersive and dissipative properties compared to their linear counterparts. For the Navier-Stokes equations, the original Vorticity Confinement method is extended up to 5th-order of accuracy with a formulation that remains independent of the choice of baseline numerical scheme. Results in the inviscid framework show that VC allows the calculation of the advection of vortices over very long distances with small dissipation. Furthermore, a preliminary study shows that it improves the prediction of large structures in the Taylor-Green Vortex flow compared to baseline FE-MUSCL schemes, but seems to reduce the dissipation of intermediate structures in the decay of turbulence even for cases where the baseline case is well-resolved. Overall, the proposed high-order VC schemes maintain the vorticity preserving capability of the original method and introduce negative dissipation according to the reduced numerical error corresponding to the increased order, enabling the use of VC in high-order simulations while preserving the accuracy order of the baseline method.

Acknowledgements

References

[1] J. G. Leishman, M. J. Bhagwat, and A. Bagai. Free-vortex filament methods for the analysis of helicopter rotor wakes. *Journal of Aircraft*, 39(5):759–775, 2002.

[2] G. Winckelmans, R. Cocle, L. Dufresne, and R. Capart. Vortex methods and their application to trailing wake vortex simulations. *Comptes Rendus Physique*, 6(4-5):467 – 486, 2005. Aircraft trailing vortices.

[3] E. Joubarne, F. Guibault, O. Braun, and F. Avellan. Numerical capture of wing tip vortex improved by mesh adaptation. *International Journal for Numerical Methods in Fluids*, 67(1):8–32, 2011.

[4] N. Hariharan, M. Steffen, A. Wissink, and M. Potsdam. Tip vortex field resolution using an adaptive dual-mesh computational paradigm. In *49th AIAA Aerospace Sciences Meeting including the New Horizons Forum and Aerospace Exposition, AIAA 2011*, volume 1108, 2011.

[5] S. J. Kamkar, A. M. Wissink, V. Sankaran, and A. Jameson. Feature-driven cartesian adaptive mesh refinement for vortex-dominated flows. *Journal of Computational Physics*, 230(16):6271–6298, 2011.

[6] M. de la Llave Plata, V. Couaillier, C. Marmignon, M.-C. Le Pape, M. Gazaix, and B. Cantaloube. Further developments in the multiblock hybrid CFD solver elsA-H. In *50th AIAA Aerospace Sciences Meeting, AIAA paper 2012-1112*, 2012.

[7] V. Sankaran, A. Wissink, A. Datta, J. Sitaraman, M. Potsdam, B. Jayaraman, A. Katz, S. Kamkar, B. Roget, D. Mavriplis, H. Saberi, W.-B. Chen, W. Johnson, and R. Strawn. Overview of the Helios version 2.0 computational platform for rotorcraft simulations. In *49th Aerospace Sciences Meeting, AIAA paper 2011-1105*. American Institute of Aeronautics and Astronautics, January 2011.

[8] G. Papadakis and S. G. Voutsinas. In view of accelerating CFD simulations through coupling with vortex particle approximations. In *Journal of Physics: Conference Series*, volume 524, page 012126. IOP Publishing, 2014.

[9] G. S. Oxley. *A 2-D Hybrid Euler-Compressible Vortex Particle Method For Transonic Rotorcraft Flows*. PhD thesis, Carleton University Ottawa, 2009.

[10] C.-W. Shu. High-order finite difference and finite volume WENO schemes and discontinuous Galerkin methods for CFD. *International Journal of Computational Fluid Dynamics*, 17(2):107–118, 2003.

[11] P. Cinnella, K. Grimich, A. Lerat, and P.-Y. Outtier. Recent progress in high-order Residual-Based Compact schemes for compressible flow simulations: Toward scale-resolving simulations and complex geometries. In *IDIHOM: Industrialization of High-Order Methods-A Top-Down Approach*, pages 397–421. Springer, 2015.

[12] K. Asthana and A. Jameson. High-order flux reconstruction schemes with minimal dispersion and dissipation. *Journal of Scientific Computing*, 62(3):913–944, 2015.

[13] K. W. Morton and P. L. Roe. Vorticity-preserving Lax-Wendroff-type schemes for the system wave equation. *SIAM Journal on Scientific Computing*, 23(1):170–192, 2001.

[14] A. Lerat, F. Falissard, and J. Sidès. Vorticity-preserving schemes for the compressible euler equations. *Journal of Computational Physics*, 225(1):635 – 651, 2007.

[15] F. Falissard, A. Lerat, and J. Sidès. Computation of airfoil-vortex interaction using a vorticity-preserving scheme. *AIAA Journal*, 46(7):1614–1623, 2008.

[16] J. Steinhoff and N. Lynn. *Treatment of vortical flows using vorticity confinement*. Chapter 10 of Computing the Future IV: Frontiers of Computational Fluid Dynamics. World Scientific, 2006.

[17] J. Steinhoff, N. Lynn, and L. Wang. *Large eddy simulation using vorticity confinement*. Chapter 4 of Implicit Large Eddy Simulations: Computing Turbulent Flow Dynamics. Cambridge University Press, 2006.

[18] J. Steinhoff, N. Lynn, W. Yonghu, M. Fan, L. Wang, and W. Dietz. *Turbulent flow simulations using vorticity confinement*. Chapter 12 of Implicit Large Eddy Simulations: Computing Turbulent Flow Dynamics. Cambridge University Press, 2006.

[19] J. Steinhoff, E. Puskas, S. Babu, Y. Wenren, and D. Underhill. Computation of thin features over long distances using solitary waves. In *13th Computational Fluid Dynamics Conference*, Snowmass, Colorado, June 1997. AIAA paper 97-1976.

[20] J. Steinhoff, W. Dietz, S. Haas, M. Xiao, N. Lynn, and M. Fan. Simulating small scale features in fluid dynamics and acoustics as nonlinear solitary waves. In *41st Aerospace Meeting and Exhibit*, Reno, Nevada, January 2003. AIAA paper 2003-078.

[21] Z. J. Wang, K. Fidkowski, R. Abgrall, F. Bassi, D. Caraeni, A. Cary, H. Deconinck, R. Hartmann, K. Hillewaert, H. T. Huynh, N. Kroll, G. May, P.-O. Persson, B. van Leer, and M. Visbal. High-order CFD methods: current status and perspective. *International Journal for Numerical Methods in Fluids*, 72(8):811–845, 2013.

[22] M. Costes and F. Juillet. Analysis and higher-order extension of the VC2 confinement scheme. *Computers & Fluids*, 56(0):102 – 117, 2012.

[23] M. Costes. Development of a 3rd-order vorticity confinement scheme for rotor wakes simulations. In

38th European Rotorcraft Forum, Amsterdam, The Netherlands, September 2012.

[24] M. Costes, I. Petropoulos, and P. Cinnella. Development of a third-order accurate vorticity confinement scheme. *Computers & Fluids*, 136:132 – 151, 2016.

[25] A. Lerat and C. Corre. *High-order residual-based compact schemes on structured grids, in CFD-Higher order discretization methods*. VKI-LS 2006-01. von Karman Institute for Fluid Dynamics, November 2006.

[26] C. Hirsch. *Numerical Computation of Internal and External Flows: The Fundamentals of Computational Fluid Dynamics: The Fundamentals of Computational Fluid Dynamics*. Butterworth-Heinemann, 2007.

[27] M. Costes. Analysis of the second vorticity confinement scheme. *Aerospace Science and Technology*, 12(3):203 – 213, 2008.

[28] M. Costes. Stability analysis of the VC2 confinement scheme for the linear transport equation. *Computers & Fluids*, 86(0):537 – 557, 2013.

[29] S. Pirozzoli. On the spectral properties of shock-capturing schemes. *Journal of Computational Physics*, 219(2):489 – 497, 2006.

[30] P.-Y. Outtier, C. Content, P. Cinnella, and B. Michel. The high-order dynamic computational laboratory for CFD research and applications. In *21st AIAA Computational Fluid Dynamics Conference*. American Institute of Aeronautics and Astronautics, June 2013.

[31] H. C. Yee, M. Vinokur, and M. J. Djomehri. Entropy splitting and numerical dissipation. *Journal of Computational Physics*, 162(1):33 – 81, 2000.

[32] G. I. Taylor and A. E. Green. Mechanism of the production of small eddies from large ones. *Proceedings of the Royal Society of London A: Mathematical, Physical and Engineering Sciences*, 158(895):499–521, 1937.

[33] J. R. Bull and A. Jameson. Simulation of the Taylor-Green vortex using high-order flux reconstruction schemes. *AIAA Journal*, 53(9):2750–2761, 2015.

[34] W. M. Van Rees, A. Leonard, D. I. Pullin, and P. Koumoutsakos. A comparison of vortex and pseudo-spectral methods for the simulation of periodic vortical flows at high reynolds numbers. *Journal of Computational Physics*, 230(8):2794–2805, 2011.

[35] C. Bogey and C. Bailly. A family of low dispersive and low dissipative explicit schemes for flow and noise computations. *Journal of Computational Physics*, 194(1):194–214, 2004.